RSC Advances

REVIEW

View Article Online
View Journal | View Issue

Cite this: *RSC Adv.*, 2020, **10**, 33879

Integration of fluorescent probes into metal–organic frameworks for improved performances

Huihui Li,[a] Weiting Yang *[ab] and Qinhe Pan *[a]

Recent years have witnessed a rapid development of fluorescent probes in both analytical sensing and optical imaging. Enormous efforts have been devoted to the regulation of fluorescent probes during their development, such as improving accuracy, sensitivity, selectivity, recyclability and overcoming the aggregation-caused quenching effect. Metal–organic frameworks (MOFs) as a new class of crystalline porous materials possess abundant host–guest chemistry, based on which they display a great application potential in regulating fluorescent probes. This review summarized the research works on the regulation of fluorescent probes using MOFs, with emphasis on the methods of integrating fluorescent probes into MOFs, the regulation effects of MOFs on fluorescent probes, the superiorities of MOFs in regulating fluorescent probes, and the outlook of this subject. It is desirably hoped that this review can provide a useful reference for the researchers interested in this field.

Received 3rd June 2020
Accepted 6th August 2020

DOI: 10.1039/d0ra04907g

rsc.li/rsc-advances

1. Introduction

In recent years, the research on fluorescent probes in both analytical sensing and optical imaging has experienced a rapid development,[1–6] encouraged by their distinctive advantages of visualization, noninvasion and facile operation. Fluorescent probes are largely constructed with fluorescent small molecules as the fluorophores in the early stage of their development,[7–9] while in the last couple of decades, there is an increasing attention on material-based fluorescent probes attributed to the emergence of various fluorescent materials.[10–12] As for the targeted analytes, they have been extended from simple ions and small molecules to biomacromolecules and even living cells,[13–16] accompanied by the number of analytes expanding to multiple substances from a single one,[17–20] which is helpful to understand more sample information and investigate the reciprocal effect of analytes.

[a]*Key Laboratory of Advanced Materials of Tropical Island Resources (Ministry of Education), School of Science, Hainan University, Haikou 570228, China. E-mail: yangwt@hainanu.edu.cn; panqinhe@163.com*

[b]*Key Laboratory of Advanced Energy Materials Chemistry (Ministry of Education), Nankai University, Tianjin 300071, China*

Huihui Li is a lecturer in School of Science, Hainan University. She received her B.S. degree in 2013 and PhD degree in 2018 both from Lanzhou University. Her current research interests focus on fluorescent porous composites and their sensing application.

Weiting Yang is a professor in School of Science, Hainan University. She received her B.S. degree in 2005, followed by PhD degree in 2010, both from Jilin University. Then she joined the group of Prof. Hongjie Zhang as a postdoctoral fellow in Changchun Institute of Applied Chemistry, Chinese Academy of Sciences, and furthermore worked there as an associate professor until 2016. Prior to joining Hainan University, she worked with Prof. Susumu Kitagawa as a specific researcher in Institute for Integrated Cell-Material Sciences, Kyoto University. Her current research interests focus on functional lanthanide nanomaterials and porous materials.

Enormous efforts have been devoted to the regulation of fluorescent probes during their development, such as improving accuracy, sensitivity, selectivity, recyclability and overcoming the aggregation-induced emission (ACQ) effect. The performances of fluorescent probes are generally improved through structural regulation, and the proposed strategies of structural regulation are as follows: (a) the accuracy can be improved by introducing two fluorophores to form the ratiometric mode;[21–23] (b) the sensitivity can be improved by using the fluorophores with high quantum yields;[24–26] (c) the selectivity can be improved by using the receptors with high specificity;[27] (d) the recyclability can be improved by using separable fluorescent materials as the fluorophores;[28–30] (e) the ACQ effect can be overcome by using the fluorophores featured with aggregation-induced emission.[31]

Metal–organic frameworks (MOFs), a class of crystalline materials composed of metal ions/clusters as nodes and organic ligands as struts, have gained significant attention in the last decade. On one hand, MOFs are equipped with the structural features of high porosity, regular channels and diverse interactions,[32–34] and on the other hand, they are characterized with multifarious properties such as fluorescence, conduction, magnetism and catalysis.[35–38] The structural features and multifarious properties endow MOFs with broad application prospects in adsorption separation, heterogeneous catalysis, drug delivery and chemical sensing.[39–42] In other perspective, the structural features of MOFs make them a class of superior host materials, and thereby, guests can be introduced to regulate the multifarious properties as well as the practical applicability of MOFs.[43–46]

The properties of guests can also be changed after being integrated into MOFs,[43–46] and on this basis, MOFs have been applied to the regulation of fluorescent probes.[47–71] MOFs exhibit the superiorities of simple operation and high efficiency compared with structural regulation, because the integration of fluorescent probes into MOFs is facile to operate,[47–71] which can improve the multiple performances of fluorescent probes simultaneously.[57,69,70] The properties of MOFs will be compromised if fluorescent probes are integrated into MOFs, thus achieving the regulation of fluorescent probes. To be specific as shown in Fig. 1, (a) the fluorescence of MOFs can serve as the second signal of ratiometric mode to improve the accuracy;[47–57] (b) the adsorption ability of MOFs can concentrate analytes near fluorescent probes to improve the sensitivity;[57–65] (c) the separation ability of MOFs can make interferents filtered out to improve the selectivity;[66,67] (d) the separability of MOFs can make fluorescent probes separable to improve the recyclability;[68–70] (e) the regular channels of MOFs can make fluorescent probes isolated to overcome the ACQ effect.[69–71]

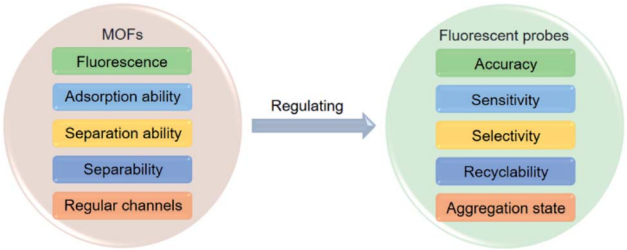

Fig. 1 Regulation effects of MOFs on fluorescent probes.

Given the above, MOFs possess a great application potential in the regulation of fluorescent probes because of their abundant host–guest chemistry. This review surveyed the research works on integrating fluorescent probes into MOFs for improved performances to provide a reference for the researchers interested in this filed. It began with the introduction of the methods for integrating fluorescent probes into MOFs. The regulation effects of MOFs on fluorescent probes were emphatically summarized in subsequent. In addition, the superiorities of MOFs in regulating fluorescent probes and the outlook of this subject were systematically discussed at the end.

2. Methods of integrating fluorescent probes into MOFs

Rare earth ion, small molecule and quantum dot (QD)-based fluorescent probes are generally integrated into MOFs.[47–71] Among various methods, *in situ* embedding[49–63,65,66,68,71] and adsorption[47,53,54,64,67,69,70] are relatively facile to operate and have little influence on the structures of guests, so fluorescent probes are commonly integrated into MOFs *via* the two methods to ensure their performances as summarized in Table 1. The detailed discussion of the two methods is presented as below in terms of operation process, application scope and characteristics. The characterization methods for the composites of fluorescent probes and MOFs are also summarized.

2.1 *In situ* embedding

In situ embedding as the most commonly used method refers to the *in situ* constructions of MOFs around the dispersed fluorescent probes as shown in Fig. 2A. It has been applied to the integration of small molecule and QD-based fluorescent probes into MOFs, such as 1-aminopyrene,[68] $CsPbBr_3$ QDs,[52] CdTe QDs,[62,66] ZnS QDs,[63] Mn^{2+}:ZnS QDs,[71] CdTe/CdS/ZnS QDs,[55] Au nanoclusters (AuNCs),[56] AgNCs,[61] CuNCs,[65] and various carbon

Qinhe Pan is a professor in School of Science, Hainan University. He received his B.S. degree in 2002 and PhD degree in 2008 both from Jilin University. After that he worked as a postdoctoral fellow in Prof. Xianhe Bu's group in Nankai University until 2010. His research interests have been focusing on the syntheses and applications of inorganic functional porous materials. Potential applications of these materials involve sensing, adsorption and separation of various chemicals.

Table 1 Summary of the research works on regulating fluorescent probes with MOFs

Fluorescent probe@MOF	Regulation effect	Method of integration	Reference
PB@UiO-66-NH_2	Accuracy	Adsorption	47
AuNCs/Cys@MIL-68(In)-NH_2	Accuracy	Covalent linkage	48
CDs@Eu-MOF	Accuracy	*In situ* embedding	49
CDs@Eu-MOF	Accuracy	*In situ* embedding	50
CDs@Eu-MOF	Accuracy	*In situ* embedding	51
$CsPbBr_3$ QDs@Eu-MOF	Accuracy	*In situ* embedding	52
CDs/Tb^{3+}@In-MOF	Accuracy	Combining two methods	53
CDs/Eu^{3+}@MOF-253	Accuracy	Combining two methods	54
QDs/CDs@ZIF-8	Accuracy	*In situ* embedding	55
AuNCs/CDs@ZIF-8	Accuracy	*In situ* embedding	56
BYCDs@ZIF-8	Accuracy/sensitivity	*In situ* embedding	57
CDs@ZIF-8	Sensitivity	*In situ* embedding	58
RhB-CDs@ZIF-8	Sensitivity	*In situ* embedding	59
CDs@ZIF-8	Sensitivity	*In situ* embedding	60
AgNCs@ZIF-8	Sensitivity	*In situ* embedding	61
CdTe QDs@ZIF-8	Sensitivity	*In situ* embedding	62
ZnS QDs@ZIF-67	Sensitivity	*In situ* embedding	63
HBDD@ZIF-8	Sensitivity	Adsorption	64
CuNCs@ZIF-8	Sensitivity	*In situ* embedding	65
CdTe QDs@ZIF-8	Selectivity	*In situ* embedding	66
CDs@UiO-66	Selectivity	Adsorption	67
1-Aminopyrene@ZIF-8	Recyclability	*In situ* embedding	68
RhB@Bio-MOF-1	Recyclability/aggregation state	Adsorption	69
Fluorescein@Cd-MOF	Recyclability/aggregation state	Adsorption	70
Mn^{2+}:ZnS QDs@ZIF-8	Aggregation state	*In situ* embedding	71

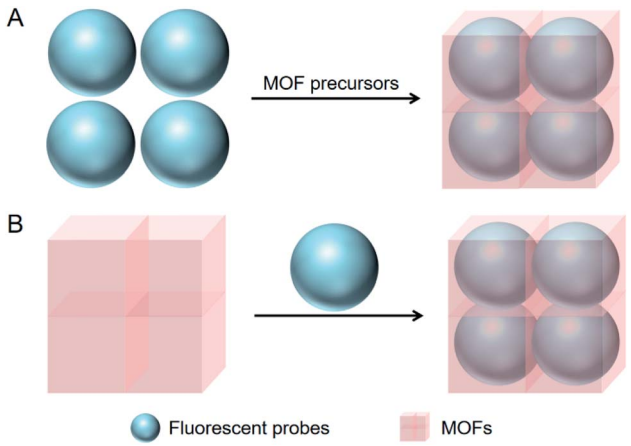

Fig. 2 Operation processes of *in situ* embedding (A) and adsorption (B).

dots (CDs).[49–51,53–57] *In situ* embedding is characterized with facile operation because the syntheses of MOFs are carried out simultaneously with the integration of fluorescent probes. For instance, 1-aminopyrene was integrated into ZIF-8 through *in situ* embedding, which was completed just by the addition of 1-aminopyrene to the mixed solution of Zn^{2+} and 2-methylimidazole (Fig. 3).[68] From another perspective, the high stability of fluorescent probes is generally required for *in situ* embedding since MOFs are commonly synthesized under the harsh conditions of long time heating. For example, the CDs prepared from Co^{2+}, tartaric acid and triethylenetetramine were integrated into an Eu-MOF through *in situ* embedding, which had to be carried out at a high temperature of 100 °C for a long time of 24 h.[49] Besides, fluorescent probes are mainly located inside the framework structures of MOFs for this method, and thus *in situ*

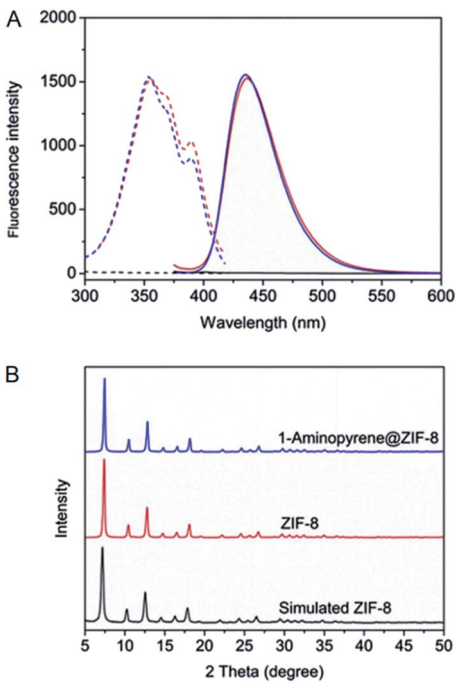

Fig. 3 (A) Excitation (dash line) and emission spectra (solid line) of ZIF-8 (black line), 1-aminopyrene@ZIF-8 (red line) and 1-aminopyrene (blue line). (B) PXRD patterns of simulated ZIF-8, ZIF-8 and 1-aminopyrene@ZIF-8. Reproduced from ref. 68 with the permission from Elsevier.

embedding is characterized with high stability and fluorescent probes are not easy to be released.[72]

2.2 Adsorption

Adsorption refers to the adsorption of fluorescent probes into the regular channels of MOFs as show in Fig. 2B, which is mainly driven by hydrogen bond, π–π stacking, electrostatic interaction and coordination interaction. It has been applied to the integration of rare earth ion, small molecule and QD-based fluorescent probes into MOFs, such as Tb^{3+},[53] Eu^{3+},[54] phloxine B (PB),[47] rhodamine B (RhB),[69] fluorescein,[70] 4,4′-(hydrazine-1,2-diylidenebis(methanylylidene)) bis(3-hydroxybenzoic acid) (HDBB),[64] and CDs.[67] Organic ligands exhibit some flexibility and coordination bonds are deformable, which results in the flexible skeletons of MOFs.[73–75] Thereby, fluorescent probes slightly larger than the channels of MOFs can also be integrated through adsorption. For instance, the size of HDBB (1.56 × 0.45 nm) was larger than the window size of ZIF-8 (0.34 nm), and nevertheless, ZIF-8 was still integrated with HDBB through adsorption ascribed to its flexible skeleton (Fig. 4).[64] Adsorption is also characterized with facile operation since it is generally carried out under mild conditions. For instance, PB was integrated into UiO-66-NH_2 through adsorption, which was completed just by dispersing UiO-66-NH_2 powder in PB solution for 2 h at room temperature.[47] From another perspective, adsorption is not so harsh for the stability of fluorescent probes due to the mild operating conditions. Additionally, fluorescent probes are mainly located on the surface of MOFs for adsorption, and this method is characterized with poor stability as a consequence.[72]

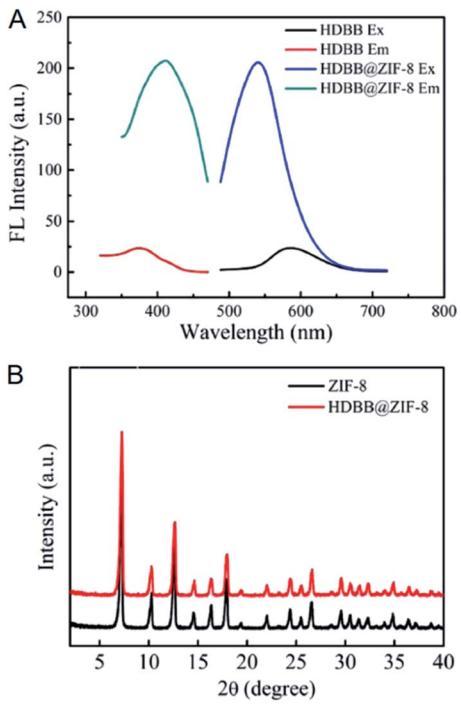

Fig. 4 (A) Excitation and emission spectra of HBDD and HBDD@ZIF-8. (B) PXRD patterns of ZIF-8 and HBDD@ZIF-8. Reproduced from ref. 64 with the permission from Elsevier.

2.3 Combing two methods

Sometimes multiple guests are simultaneously integrated into MOFs, for instance, a fluorescent probe is integrated into a MOF together with a reference fluorophore or another fluorescent probe to form the ratiometric mode.[53–57] In such situation, *in situ* embedding and adsorption may be employed in combination owing to the different properties of guests. For instance, the CDs prepared from citric acid and ethylenediamine were integrated into MOF-253 together with Eu^{3+} for the ratiometric detection of Hg^{2+}, and in this case, the CDs and Eu^{3+} were respectively integrated through *in situ* embedding and adsorption (Fig. 5).[54] In addition, the CDs prepared from *p*-phenylenediamine were integrated into an In-MOF together with Tb^{3+} for the ratiometric detection of water in organic solvents, in which case the CDs and Tb^{3+} were integrated *via in situ* embedding and adsorption, respectively.[53]

Above all, *in situ* embedding and adsorption are the two most common methods used for integrating fluorescent probes into MOFs, and their operation processes are both very facile. Compared with *in situ* embedding, adsorption is carried out under milder conditions and is not so harsh for the stability of fluorescent probes. However, adsorption requires that fluorescent probes are not much larger than the channels of MOFs, while this is not necessary for *in situ* embedding. As for stability,

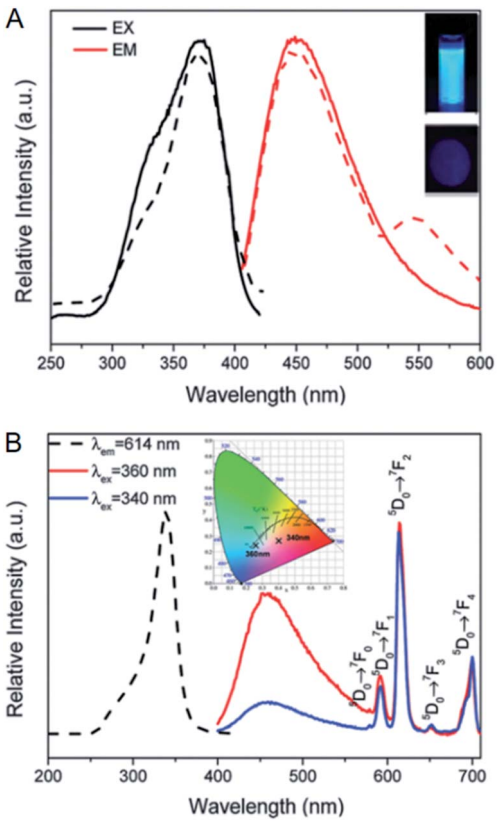

Fig. 5 (A) Excitation and emission spectra of CDs@MOF-253 in the aqueous solution (solid line) and in the solid state (dash line). (B) Excitation (dash line) and emission (solid line) spectra of CDs/Eu^{3+}@MOF-253. Reproduced from ref. 54 with the permission from Royal Society of Chemistry.

in situ embedding is more superior compared with adsorption because fluorescent probes are located deeper into the framework structures of MOFs. Our group has done some research on integrating fluorescent guests into MOFs for chemical sensing recently.[46,68] It is found that most fluorescent guests are left in solutions for the two methods, so how to improve the utilization of fluorescent guests is an issue needing to be overcome in future. Enhancing the interactions of MOFs with fluorescent guests through the modification of MOFs is an alternative strategy to overcome the above issue.

2.4 Characterization methods

The integration of fluorescent probes into MOFs can be confirmed by comparing the fluorescence spectra, FTIR spectra or specific surface areas of MOFs before and after the integration. If fluorescent probes and MOFs are integrated together, the characteristic emission bands of fluorescent probes will be observed in fluorescence spectra,[47–71] and the characteristic absorption bands of fluorescent probes will appear in FTIR spectra,[47,49–51,53,55,56,58,60,63,64,67,71] and there will be a certain level of decline in specific surface areas.[47,50,51,53,54,58,63,64,67,70,71] TEM is also an available tool to confirm the integration for QD-based fluorescent probes, and the small spots of fluorescent probes may be observed if fluorescent probes are integrated into MOFs.[48,52,57,62,63,65,66] In addition, there are two strategies for determining the loading amounts of fluorescent probes in MOFs. One is monitoring the residual amounts of fluorescent probes after the integration with MOFs,[69,70] and the other is monitoring the released amounts of fluorescent probes after the decomposition of MOFs.[64,68,71] Besides, the distribution of fluorescent probes in MOFs can be observed with confocal laser scanning microscope.[64,70] Additionally, PXRD and TEM/SEM can be used to evaluate the crystalline structures and morphologies of the composites of fluorescent probes and MOFs, respectively.[47–71] Moreover, the quantum yields of the composites and pristine fluorescent probes are sometimes determined to investigate the influence of MOFs on the emission of fluorescent probes.[62,65,68]

3. Regulation effects of MOFs on fluorescent probes

MOFs possess fluorescence, adsorption ability, separation ability, separability and regular channels. These properties will be compromised if fluorescent probes are integrated into MOFs, and the regulation effects of MOFs on fluorescent probes are realized on this basis, which haven been summarized in Table 1: (a) accuracy regulation,[47–57] (b) sensitivity regulation,[57–65] (c) selectivity regulation,[66,67] (d) recyclability regulation,[68–70] and (e) aggregation state regulation.[69–71] The discussion of each regulation effect is presented as below in terms of mechanism and research works.

3.1 Accuracy regulation

Traditional fluorescent probes, only possessing one emission band, determine the concentrations of analytes according to the change of fluorescence intensity at a single wavelength.[76–78] Nevertheless, the accuracy of their detection results is easily influenced by external parameters such as environment and instrumentation. Ratiometric fluorescent probes with two emission bands are therewith developed in order to overcome the above issue, which measure the fluorescence intensities at two different wavelengths and use the ratio as the characteristic parameter to detect the analytes.[79–81] MOFs commonly possess fluorescence that can be originated from metal ions,[82] organic ligands[83,84] or guests,[85] which makes them available to regulate the accuracy of fluorescent probes. That is to say, the fluorescence of MOFs can serve as the second signal of ratiometric mode when fluorescent probes and MOFs are integrated together, thus improving the accuracy of fluorescent probes.[47–57]

There have been four strategies proposed to endow fluorescent probes with ratiometric mode *via* MOFs. The first strategy is integrating a fluorescent probe into a fluorescent MOF that serves as the reference fluorophore. The fluorescence intensity of the fluorescent probe is changed while the MOF displays the original fluorescence intensity after adding the analyte (Fig. 6A).[47–49] The second strategy is integrating a fluorescent probe into a fluorescent MOF which also responds to the analyte. The fluorescence intensity of the fluorescent probe is changed while the MOF displays an opposite change in fluorescence intensity after adding the analyte (Fig. 6B).[50–52] The third strategy is integrating a fluorescent probe and a reference fluorophore into a MOF. The fluorescent intensity of the fluorescent probe is changed while the reference fluorophore displays the original fluorescence intensity after adding the analyte (Fig. 6C).[53–56] The fourth strategy is integrating two

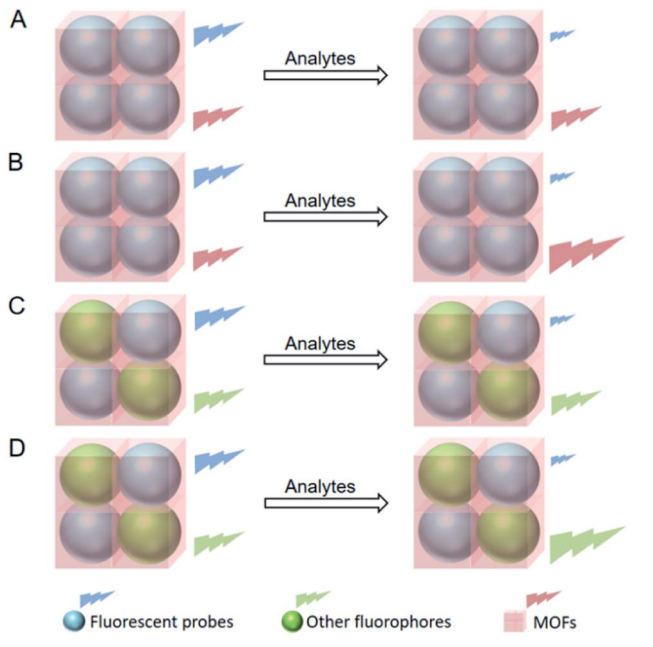

Fig. 6 Proposed strategies to endow fluorescent probes with ratiometric mode through MOFs, (A) fluorescent MOFs display no response, (B) fluorescent MOFs display opposite response, (C) other fluorophores display no response, (D) other fluorophores display opposite response.

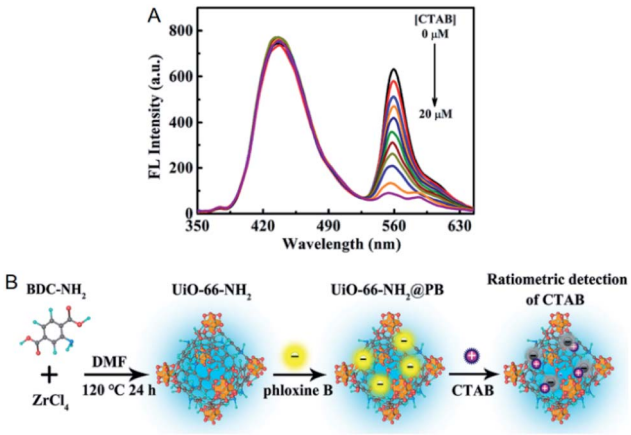

Fig. 7 (A) Fluorescence signal changes of PB@UiO-66-NH_2 after the addition of CTAB. (B) Mechanism for the ratiometric detection of CTAB with PB@UiO-66-NH_2. Reproduced from ref. 47 with the permission from American Chemical Society.

fluorescent probes which are targeted at the same analyte into a MOF. The fluorescence intensities of the two fluorescent probes are all changed while their changing trends are opposite after adding the analyte (Fig. 6D).[57]

For the examples of the first strategy (Fig. 6A), the yellow-emitting PB was integrated into the blue-emitting UiO-66-NH_2 for the ratiometric detection of cetyltrimethyl ammonium bromide (CTAB).[47] In the presence of CTAB, the fluorescence of PB was quenched owing to the electronic interaction between CTAB and PB, while UiO-66-NH_2 acting as the reference fluorophore displayed the original fluorescence intensity (Fig. 7). Based on this, CTAB was quantified in the concentration range from 0.1 to 17 μM with a detection limit of 0.074 μM. Furthermore, CTAB in water samples collected from tap and river was detected with spiked recoveries ranging from 94 to 114%.

Besides, the red-emitting AuNCs capped with glutathione (GSH) was integrated into the blue-emitting MIL-68(In)-NH_2 followed by L-cysteine (Cys) modification for the ratiometric detection of Hg^{2+}.[48] The fluorescence intensity of AuNCs/Cys was decreased after the addition of Hg^{2+}, while MIL-68(In)-NH_2 acting as the reference fluorophore was not influenced by Hg^{2+}. Based on the fluorescence intensity ratio, Hg^{2+} was quantified in the concentration range from 20 pM to 60 μM with a detection limit of 6.7 pM. Furthermore, Hg^{2+} in water samples collected from tap and lake was detected with spiked recoveries ranging from 96.4 to 110.2%. Radial star-shaped test strips were further fabricated, and the fluorescence color turned from red to blue when Hg^{2+} was added.

Additionally, the blue-emitting CDs prepared from Co^{2+}, tartaric acid and triethylenetetramine were integrated into the red-emitting Eu-MOF for the ratiometric detection of $Cr_2O_7^{2-}$.[49] In the presence of $Cr_2O_7^{2-}$, the fluorescence of CDs was quenched owing to the inner filter effect (IFE), while Eu-MOF as the reference fluorophore displayed the original fluorescence intensity. Based on the fluorescence intensity ratio, $Cr_2O_7^{2-}$ was quantified in the concentration range from 2 to 100 μM, and the limit of detection was calculated to be 0.21 μM. Furthermore, $Cr_2O_7^{2-}$ in water samples collected from tap, river and steam

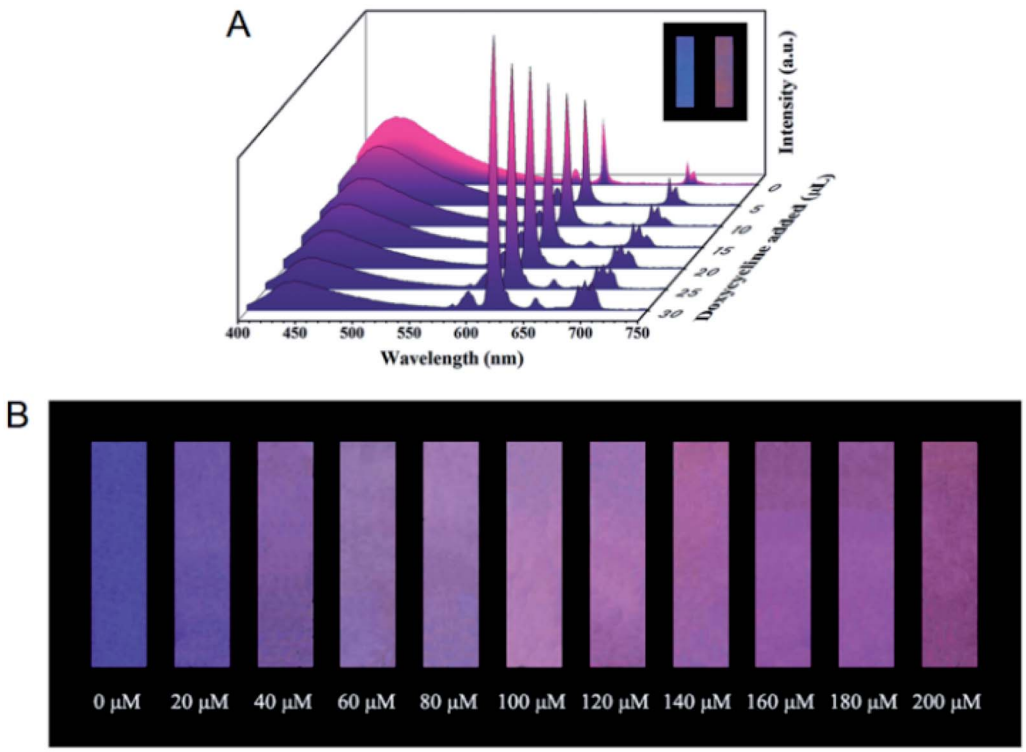

Fig. 8 (A) Fluorescence signal changes of CDs@Eu-MOF after the addition of doxycycline. (B) Fluorescence color change of the test strip after the addition of doxycycline. Reproduced from ref. 50 with the permission from Royal Society of Chemistry.

was detected with spiked recoveries in the range of 91.90–110.62%.

For the examples of the second strategy (Fig. 6B), the blue-emitting CDs prepared from citric acid and ethylene diamine were integrated into the red-emitting Eu-MOF for the ratiometric detection of doxycycline.[50] In the presence of doxycycline, the fluorescence of CDs was quenched owing to the overlap between the absorption band of doxycycline and the emission band of CDs, while Eu-MOF displayed increased fluorescence intensity attributed to the formation of Eu–doxycycline complex (Fig. 8A). Doxycycline was quantified in the concentration range from 0 to 60 μM with the limit of detection of 0.36 μM based on the fluorescence intensity ratio. Furthermore, the concentration of doxycycline in a simulated biological system was measured, and the spiked recoveries were obtained ranging from 93.95 to 102.28%. Moreover, test strips were fabricated for the convenience of use, and the fluorescence color changed from blue to red after adding doxycycline (Fig. 8B).

Besides, the blue-emitting CDs prepared from citric acid and Cys were integrated into the red-emitting Eu-MOF for the ratiometric detection of water in organic solvents.[51] As the water content in organic solvents increased, CDs changed from the aggregated state to the dispersed state accompanied by fluorescence enhancement, while Eu-MOF displayed fluorescence quenching owing to the effect of O–H oscillators. The water content in ethanol was quantified in the range from 0.05 to 4% with a detection limit of 0.03% based on the fluorescence intensity ratio. The water contents in other organic solvents such as *N*,*N*-dimethylformamide and acetonitrile could also be determined.

Additionally, the green-emitting $CsPbBr_3$ QDs were integrated into the red-emitting Eu-MOF for the ratiometric detection of temperature.[52] As temperature increased from 20 to 100 °C, the fluorescence of $CsPbBr_3$ QDs was quenched while Eu-MOF displayed increased fluorescence intensity. The relationship between the fluorescence intensity ratio and the temperature could be described by the equation of $I_{MOF}/I_{QD} = -0.536 + 1.422 \times e^{0.031T}$. In addition, the fluorescence intensity ratio could display a reversible transformation with the change of temperature.

For the examples of the third strategy (Fig. 6C), the red-emitting CDs prepared from *p*-phenylenediamine were integrated into an In-MOF together with the green-emitting Tb^{3+} for the ratiometric detection of water in organic solvents.[53] As the water content in organic solvents increased, CDs turned from the aggregation state to the dispersion state along with fluorescence enhancement, while Tb^{3+} acting as the reference fluorophore displayed the original fluorescence intensity (Fig. 9A and B). Based on this, the water contents in ethanol, *N*,*N*-dimethylformamide and cyclopropane were quantified in the ranges of 0–30%, 0–30% and 0–40% with detection limits of 0.28%, 0.33% and 0.25%, respectively. Test strips were further fabricated for the detection of humidity, and the fluorescence color changed from red to green when humidity increased (Fig. 9C).

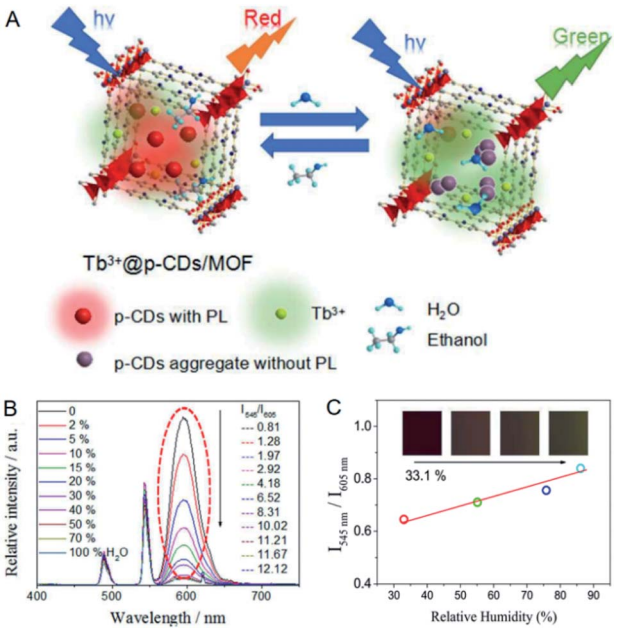

Fig. 9 (A) Mechanism for the ratiometric detection of water in organic solvents with CDs/Tb^{3+}@In-MOF. (B) Fluorescence signal changes of CDs/Tb^{3+}@In-MOF with increasing the water content in ethanol. (C) Fluorescence signal changes of the test strip with the increase of humidity. Reproduced from ref. 53 with the permission from Royal Society of Chemistry.

Besides, the blue-emitting CDs prepared from citric acid and ethylenediamine were integrated into MOF-253 together with the red-emitting Eu^{3+} for the ratiometric fluorescent detection of Hg^{2+}.[54] In the presence of Hg^{2+}, the fluorescence of CDs was quenched owing to the coordination between Hg^{2+} and the functional groups of CDs, while Eu^{3+} serving as the reference fluorophore displayed the original fluorescence intensity. Hg^{2+} was quantified in the concentration range from 0.065 to 150 μM based on the fluorescence intensity ratio, and the limit of detection for Hg^{2+} was calculated to be 13 ppb. Furthermore, Hg^{2+} in water samples collected from tap, river and fountain was measured, and the spiked recoveries were determined ranging from 96.2 to 102.6%.

Additionally, the red-emitting CdTe/CdS/ZnS QDs were integrated into ZIF-8 together with the blue-emitting CDs prepared from citric acid and diethylene triamine for the ratiometric detection of Cu^{2+}.[55] In the presence of Cu^{2+}, the Cd^{2+} in CdTe/CdS/ZnS QDs was replaced to generate the low soluble CuTe, which resulted in fluorescence quenching, whereas CDs serving as the reference fluorophore displayed the original fluorescence intensity. Based on this, Cu^{2+} was quantified in the concentration range from 5 to 100 nM with a detection limit of 1.53 nM. Furthermore, Cu^{2+} in tap water was determined with spiked recoveries ranging from 94.4 to 105.0%.

In addition, the red-emitting AuNCs capped by GSH were integrated into ZIF-8 together with the blue-emitting CDs prepared from sodium citrate and tripolycyanamide for the ratiometric detection of Cu^{2+}.[56] The fluorescence of the AuNCs was quenched in the presence of Cu^{2+} owing to the coordination

between Cu^{2+} and GSH, and nevertheless, Cu^{2+} had little influence on the fluorescence intensity of the CDs which acted as the reference fluorophore. Cu^{2+} was quantified in the concentration range from 0.001 to 1000 μM based on the fluorescence intensity ratio, and moreover, the limit of detection for Cu^{2+} was calculated to be 0.3324 nM. Furthermore, the concentration of Cu^{2+} in serum samples was determined, and the spiked recoveries were obtained ranging from 95.6 to 104.5%.

For the examples of the fourth strategy (Fig. 6D), the yellow-emitting CDs (YCDs) prepared from *o*-phenylenediamine were integrated into ZIF-8 together with the blue-emitting CDs (BCDs) prepared from urea and citric acid for the ratiometric detection of GSH.[57] The fluorescence of the YCDs was enhanced in the presence of Cu^{2+} ascribed to the coordination of Cu^{2+} with *o*-phenylenediamine residues, while the BCDs displayed fluorescence quenching after the addition of Cu^{2+} as their emission band was overlapped by the absorption band of Cu^{2+}-*o*-phenylenediamine complex. When GSH was added further, the fluorescence changes as described above were inhibited ascribed to the strong coordination of GSH with Cu^{2+} (Fig. 10A). GSH was quantified in the concentration range of 3–25 nM with a detection limit of 0.9 nM on this basis. Furthermore, GSH in fruit samples collected from grape and cucumber was detected with spiked recoveries ranging from 97.2 to 106.3%.

3.2 Sensitivity regulation

MOFs possess the structural characteristics of high porosity, regular channels and diverse interactions, and consequently

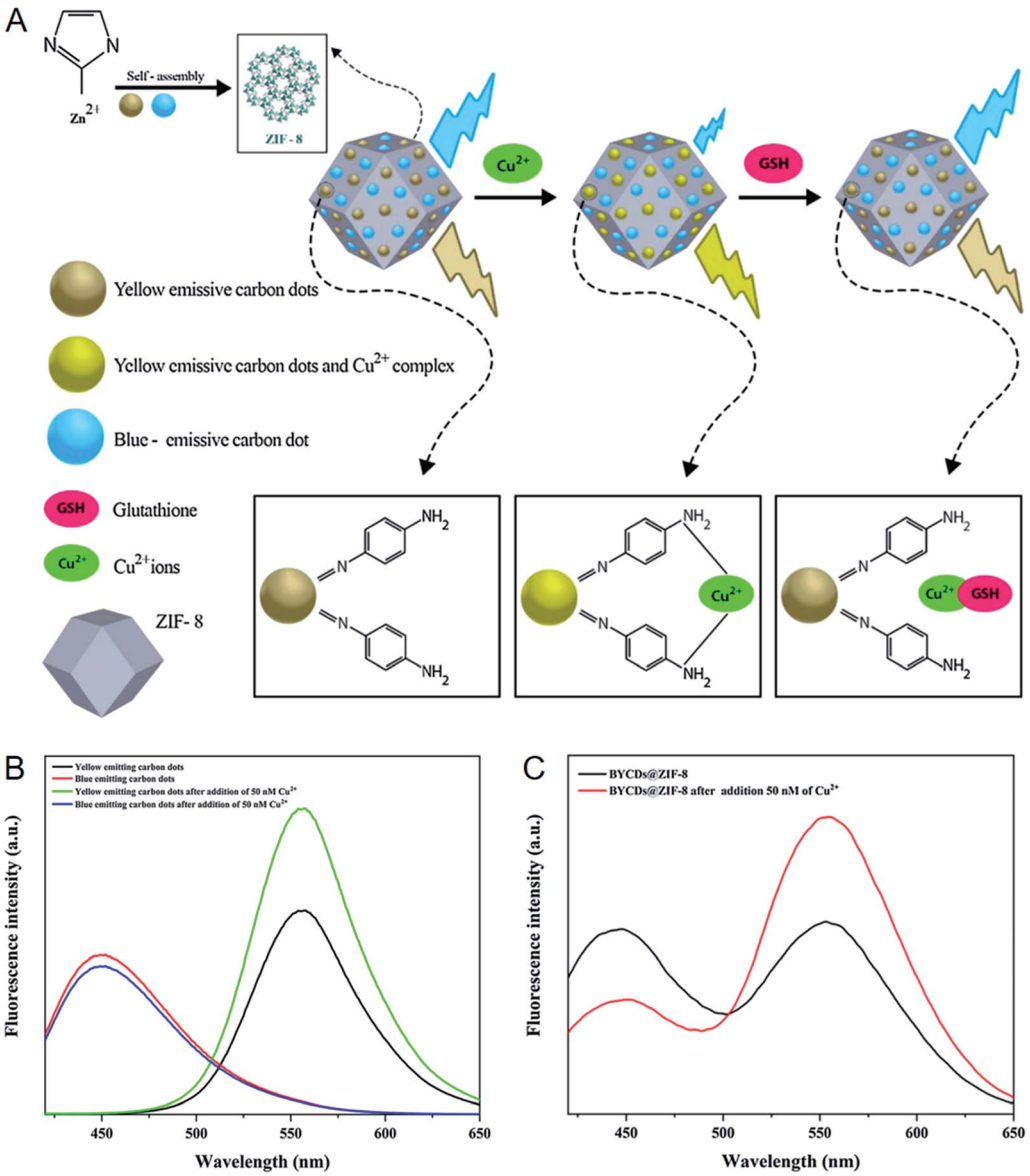

Fig. 10 (A) Mechanism for the ratiometric detection of GSH with BYCDs@ZIF-8. (B) Fluorescence signal changes of BCDs and YCDs after the addition of Cu^{2+}. (C) Fluorescence signal changes of BYCDs@ZIF-8 after the addition of Cu^{2+}. Reproduced from ref. 57 with the permission from Elsevier.

they have a broad application prospect in the field of adsorption.[86–88] The adsorption ability of MOFs makes them available for the sensitivity regulation of fluorescent probes.[57–65] To be specific, the analytes can be concentrated by MOFs to the vicinity of fluorescent probes when fluorescent probes and MOFs are integrated together, so as to improve the sensitivity of fluorescent probes. ZIF-8, composed of Zn^{2+} and 2-methylimidazole, is the most commonly used MOF to regulate the sensitivity of fluorescent probes attributed to its facile preparation and excellent stability besides superior adsorption ability.[89–93] Fluorescent probes based on various CDs, HBDD and CuNCs have been integrated into ZIF-8 to realize the improvement of sensitivity.[57–64]

The CDs prepared from *N*-(β-aminoethyl)-γ-aminopropyl methyldimethoxysilane were integrated into ZIF-8 for the sensitive detection of quercetin.[58] The fluorescence of the CDs was quenched after the addition of quercetin owing to the overlap between the excitation band of the CDs and the absorption band of quercetin. It was found that the CDs displayed improved quenching efficiency after integrated into ZIF-8 under the same condition, which could be explained by the adsorption of quercetin by ZIF-8 according to the adsorption experiment (Fig. 11). As a result, quercetin was quantified in the concentration range of 0.01–50.0 μM with a detection limit as low as 3.5 nM. Furthermore, the concentration of quercetin in red wine was determined, and the result (8.44 ± 0.062 μM) was consistent with that from HPLC-UV method (8.41 ± 0.054 μM).

RhB modified CDs were integrated into ZIF-8 for the ratiometric detection of HClO.[59] RhB was oxidized after the addition of HClO accompanied by fluorescence quenching, while HClO exhibited little effect on the fluorescence intensity of CDs serving as the reference fluorophore. Noteworthily, RhB displayed higher quenching efficiency after integrated into ZIF-8 under the same condition, and the authors attributed this phenomenon to the adsorption ability of ZIF-8 toward HClO. As a consequence, HClO was quantified in the concentration range from 15 to 180 μM, and moreover, the limit of detection for HClO was calculated as low as 6.7 μM. In addition, HClO in the commercial disinfectant was detected with spiked recoveries ranging from 95.4 to 106.0%.

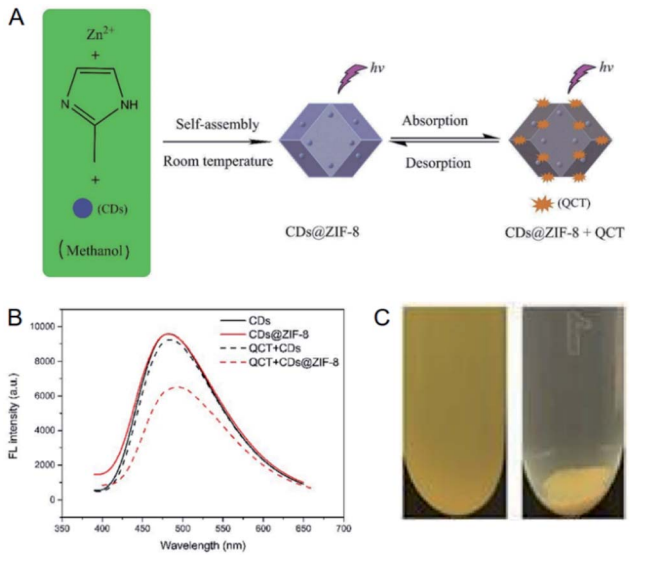

Fig. 11 (A) Mechanism for the sensitive detection of quercetin with CDs@ZIF-8. (B) Comparison of the responses of CDs and CDs@ZIF-8 toward quercetin. (C) Paragraphs of CDs@ZIF-8 suspended in quercetin solution before (left) and after (right) centrifugation. Reproduced from ref. 58 with the permission from Royal Society of Chemistry.

The CDs prepared from citric acid and poly(ethylenimine) were integrated into ZIF-8 for the sensitive detection of Cu^{2+}.[60] The fluorescence of the CDs was quenched after the addition of Cu^{2+} owing to the interaction of Cu^{2+} with poly(ethylenimine). It was found that the CDs displayed higher quenching efficiency after integrated into ZIF-8 under the same condition, and the adsorption experiment confirmed that this phenomenon was owing to the adsorption of Cu^{2+} by ZIF-8. As a consequence, Cu^{2+} was quantified in the concentration range from 2 to 1000 nM, and the detection limit for Cu^{2+} was calculated as low as 80 pM. Furthermore, the concentration of Cu^{2+} in river water was determined, and the result (2.201 ± 0.084 μM) was consistent with that obtained from ICP-MS method (2.164 ± 0.052 μM). In subsequent, fluorescent probes based on other CDs, AgNCs and CdTe QDs were integrated into ZIF-8 to achieve the sensitive detection of Cu^{2+}.[57,61,62]

ZIF-67, consisted of Co^{2+} and 2-methylimidazole, belongs to the same family of MOFs as ZIF-8, and possesses the adsorption ability toward Cu^{2+} as well.[94] The ZnS QDs capped with polyethylene glycol were integrated into ZIF-67 for the sensitive detection of Cu^{2+}.[63] The fluorescence of ZnS QDs was quenched after the addition of Cu^{2+} attributed to the interaction between Cu^{2+} and polyethylene glycol. The quenching efficiency of ZnS QDs was increased after integrated into ZIF-8 under the same condition, and this phenomenon was caused by the adsorption of Cu^{2+} by ZIF-67 according to the adsorption experiment. As a consequence, Cu^{2+} was quantified in the concentration range from 3 to 500 nM with a detection limit as low as 0.96 nM. Furthermore, the concentration of Cu^{2+} in tap water was determined and the spiked recoveries were ranging from 99.5 to 102.0%.

HDBB was integrated into ZIF-8 with a loading amount of 0.8 wt% for the sensitive detection of ethanol in water.[64] The fluorescence intensity of HBDD was enhanced slowly with increasing the ethanol content in water, which could be explained by the solvent effect. Nevertheless, HBDD displayed drastic fluorescence enhancement after integrated into ZIF-8 under the same condition, and this phenomenon was ascribed to the adsorption of ethanol by ZIF-8 as demonstrated in literature.[95] As a consequence, the ethanol content in water could be quantified in the range from 10 to 90% with a detection limit as low as 2.16%. In addition, the fluorescence was reversibly switched between the weak and strong status with the change of the ethanol content in water.

The CuNCs capped with polyethyleneimine were integrated into ZIF-8 for the sensitive detection of H_2O_2.[65] The quantum yields of CuNCs increased from 0.12 to 1.8% after the integration with ZIF-8, which was due to the formation of aggregates. The fluorescence of CuNCs was quenched in the presence of

H_2O_2 owing to the H_2O_2-induced oxidation of Cu to Cu^{2+}. The result showed that CuNCs exhibited higher quenching efficiency after integrated into ZIF-8 under the same condition, and the authors attributed this phenomenon to the adsorption ability of ZIF-8 toward H_2O_2. On this basis, H_2O_2 was quantified in the concentration range from 0.01 to 1.5 μM with a detection limit as low as 10 nM. Furthermore, the activity of glucose oxidase was measured through the detection of H_2O_2.

3.3 Selectivity regulation

As mentioned above, the structural characteristics of MOFs make them possess superior adsorption ability.[86–88] Based on this, the analytes can be concentrated by MOFs to the vicinity of fluorescent probes when fluorescent probes and MOFs are integrated together, so as to improve the sensitivity of fluorescent probes.[57–65] Generally speaking, substances display discrepant adsorption on MOFs because of their different functional groups, molecule sizes or chiral structures, and therefore MOFs possess the ability to separate different substances.[96–98] In other perspective, the separation ability of MOFs makes them available to regulate the selectivity of fluorescent probes.[66,67] That is to say, the interferents can be filtered out by MOFs when fluorescent probes and MOFs are integrated together, thus improving the selectivity of fluorescent probes. Fluorescent probes based on CdTe QDs and CDs have been integrated into MOFs to achieve the improvement of their selectivity.[66,67]

CdTe QDs were integrated into ZIF-8 for the selective measurement of oxidase activities based on H_2O_2 detection (Fig. 12A).[66] CdTe QDs could be applied to detecting H_2O_2 based on the oxidation-induced fluorescence quenching, while oxidases and substates also exhibited effects on the fluorescence intensity of CdTe QDs (Fig. 12B). Smaller H_2O_2 could readily enter the cage windows of ZIF-8, while oxidases and substates with large sizes would be obstructed. As a result, only H_2O_2 permeated ZIF-8 to induce the fluorescence quenching of CdTe QDs and the interferences from oxidases and substates were eliminated when CdTe QDs and ZIF-8 were integrated together (Fig. 12C). Based on this, the activities of GOx and urate oxidases (UOx) were selectively measured in the ranges of 1–100 and 0.1–50 U L^{-1} with detection limits of 0.26 and 0.024 U L^{-1}, respectively.

The CDs prepared from citric acid and ethylenediamine were integrated into UiO-66 for the selective detection of 4-nitrophenol.[67] The CDs could be applied to detecting 4-nitrophenol based on fluorescence quenching, whereas they suffered from the interferences from 2,4-dinitrophenol and 2,4,6-trinitrophenol. UiO-66 possessed much higher adsorption capacity toward 4-nitrophenol (17.3 mg g^{-1}) compared with 2,4-dinitrophenol (1.8 mg g^{-1}) and 2,4,6-trinitrophenol (1.3 mg g^{-1}) according to the adsorption experiment. As a consequence, only 4-nitrophenol permeated UiO-66 to induce the fluorescence quenching of the CDs and the interferences from 2,4-dinitrophenol and 2,4,6-trinitrophenol were diminished when the CDs and UiO-66 were integrated together. On this basis, 4-nitrophenol was selectively detected in the concentration range from 0.01 to 20.0 μM, and moreover, the limit of detection for 4-nitrophenol was calculated to be 3.5 nM.

3.4 Recyclability regulation

The recycle of fluorescent probes is helpful to reduce the cost in practical applications. One of the important factors for

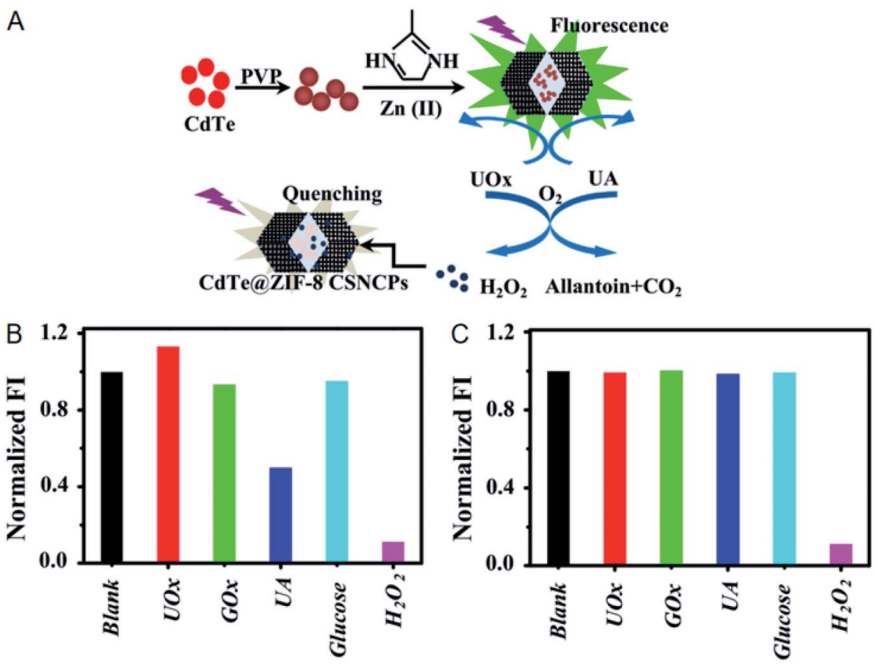

Fig. 12 (A) Mechanism for the selective measurement of oxidase activities with CdTe QDs@ZIF-8. (B) Fluorescence intensities of CdTe QDs in the presence of different substances. (C) Fluorescence intensities of CdTe QDs@ZIF-8 in the presence of different substances. Reproduced from ref. 66 with the permission from Elsevier.

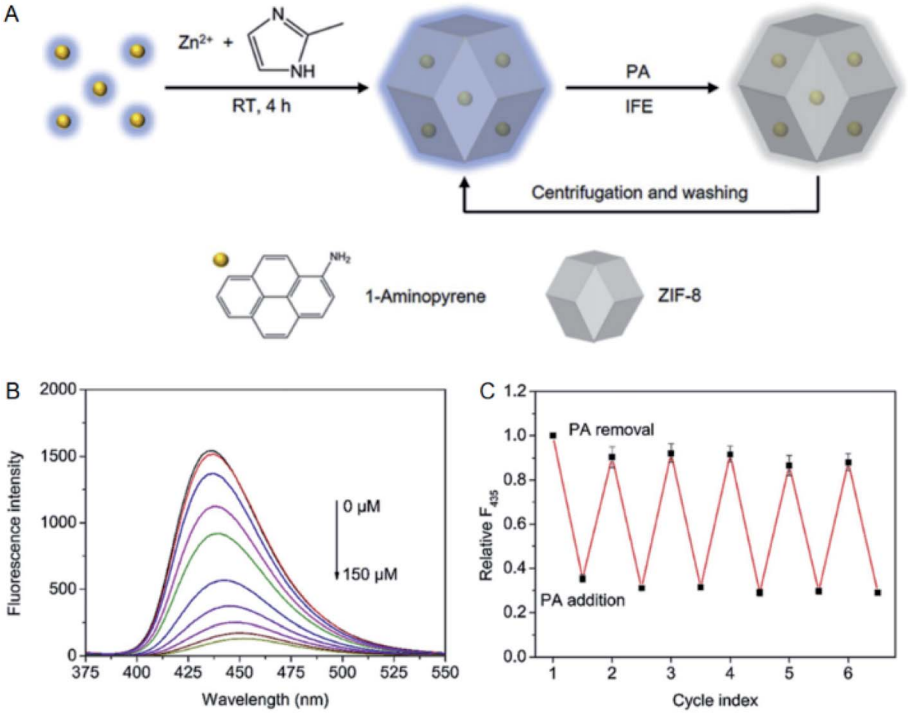

Fig. 13 (A) Mechanism for the recyclable detection of PA with 1-aminopyrene@ZIF-8. (B) Fluorescence titration of 1-aminopyrene@ZIF-8 with PA. (C) Recycle test of 1-aminopyrene@ZIF-8 for the detection of PA. Reproduced from ref. 68 with the permission from Elsevier.

recycling fluorescent probes is separability. Apparently, MOF-based fluorescent probes satisfy this requirement and commonly possess excellent recyclability, and our groups have developed a series of recyclable fluorescent probes based on MOFs.[99–101] By contrast, the recyclability of other fluorescent probes such as the ones based on small molecules and QDs is generally poor, and one of the important reasons is the difficulty to separate them from the detection systems.[102–105] The separability of MOFs makes them available to regulate the recyclability of fluorescent probes.[68–70] To be specific, fluorescent probes can follow MOFs to be separated from the detection systems when fluorescent probes and MOFs are integrated together, thus improving the recyclability of fluorescent probes. Fluorescent probes based on 1-aminopyrene, RhB and fluorescein have been integrated into MOFs to achieve the improvement of their recyclability.[68–70]

For instance, our group integrated 1-aminopyrene into ZIF-8 with a loading amount of 1.4 mg g^{-1} for the recyclable detection of picric acid (PA) more recently.[68] There exhibits no obvious distinction between the quantum yields of 1-aminopyrene before (10.7%) and after (11.1%) the integration with ZIF-8. The fluorescence of 1-aminopyrene was quenched in the presence of PA attributed to IFE, and the recyclable detection of PA was realized with the assistance of ZIF-8 (Fig. 13). In addition, PA was quantified in the concentration range from 1 to 150 μM, and the limit of detection for PA was calculated to be 0.3 μM. Furthermore, PA in water samples collected from lake and sea was measured, and the spiked recoveries were determined ranging from 96.0 to 104.0%.

3.5 Aggregation state regulation

Most fluorophores suffer from the ACQ effect and their fluorescence is quenched in the solid state, which is not conducive to develop detection devices such as test strips with relevant fluorescent probes. The regular channels of MOFs make them available to avoid the ACQ effect of fluorescent probes through aggregation state regulation.[69–71] That is to say, fluorescent probes can be isolated in the regular channels of MOFs when fluorescent probes and MOFs are integrated together, thus regulating the aggregation state and avoiding the ACQ effect. Noteworthily, the loading amounts of fluorescent probes in MOFs have to be controlled in a certain range since high loading amounts may cause fluorescent probes to form aggregates.[106] Fluorescent probes based on RhB, fluorescein and Mn^{2+}:ZnS QDs have been integrated into MOFs to realize the aggregation state regulation.[69–71]

For instance, Mn^{2+}:ZnS QDs were integrated into ZIF-8 with a loading amount of 1.6 wt% to regulate the aggregation state.[71] As expected, Mn^{2+}:ZnS QDs displayed stronger fluorescence in the solid state after integrated into ZIF-8 ascribed to the regular channels (Fig. 14A). In addition, Co^{2+} and $Cr_2O_7^{2-}$ were both detected in the concentration range from 0 to 100 μM based on fluorescence quenching (Fig. 14B and C). Moreover, the limits of detection for Co^{2+} and $Cr_2O_7^{2-}$ were calculated to be 0.27 and 0.22 μM, respectively. Furthermore, Co^{2+} in human serum and $Cr_2O_7^{2-}$ in tap water were detected with spiked recoveries in the ranges of 98.87–100.35% and 99.79–105.07%, respectively.

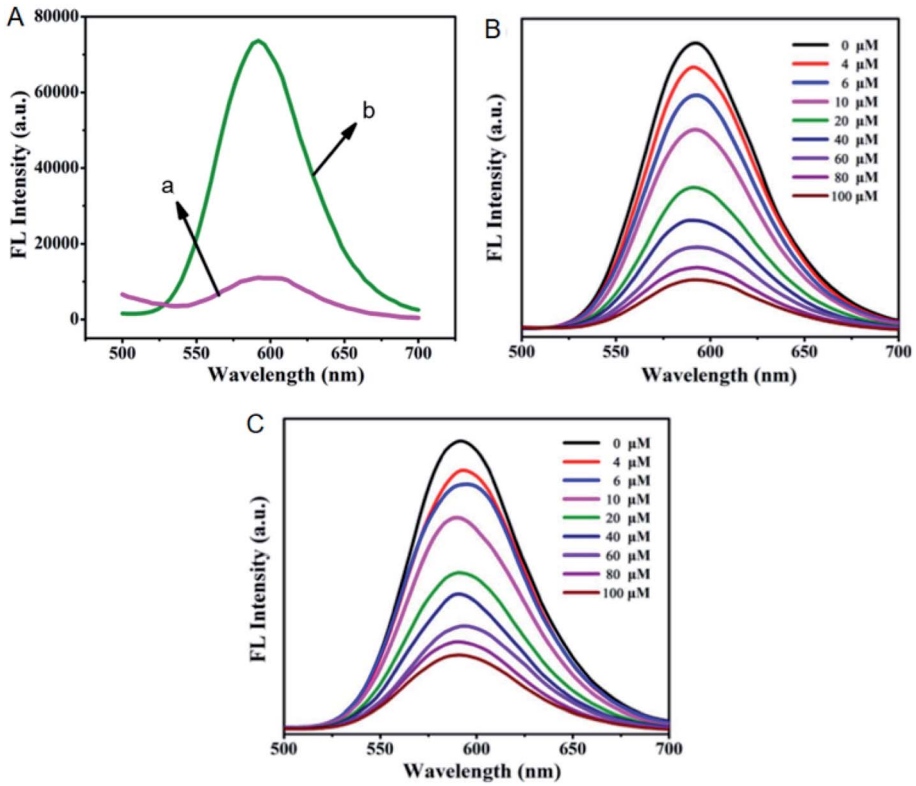

Fig. 14 (A) Emission spectra of solid Mn^{2+}:ZnS QDs (a) and solid Mn^{2+}:ZnS QDs@ZIF-8 (b). (B) Fluorescence titration of Mn^{2+}:ZnS QDs@ZIF-8 with Co^{2+}. (C) Fluorescence titration of Mn^{2+}:ZnS QDs@ZIF-8 with $Cr_2O_7^{2-}$. Reproduced from ref. 71 with the permission from Elsevier.

4. Superiorities of MOFs in regulating fluorescent probes

The conventional strategy to improve the performances of fluorescent probes is structural regulation, in which the fluorophores or receptors are selected elaborately. Structure regulation usually improves one performance of fluorescent probes at the same time.[21–31] By contrast, fluorescent probes are regulated with MOFs based on host–guest chemistry, which can improve the multiple performances of fluorescent probes simultaneously.[57,69,70] Therefore, MOFs display the superiority of high efficiency compared with structural regulation. For instance,[57] the ratiometric detection of Cu^{2+} was realized through the integration of YCDs and BCDs into ZIF-8 (Fig. 10A). Meanwhile, YCDs and BCDs displayed enhanced sensitivity toward Cu^{2+} due to the adsorption ability of ZIF-8 (Fig. 10B and C). Therefore, the accuracy and sensitivity were both improved in this work. In addition, the synthetic routes of fluorescent probes have to be reexplored in structural regulation,[21–31] while the methods of integrating fluorescent probes into MOFs are commonly facile to operate.[47,49–71] Hence, MOFs also exhibit the superiority of simple operation compared with structural regulation.

5. Conclusions and outlook

In summary, this review summarized the research works on the regulation of fluorescent probes with MOFs. The regulation effects of MOFs on fluorescent probes including accuracy, selectivity, sensitivity, recyclability and aggregation state were highlighted. In addition, the methods of integrating fluorescent probes into MOFs and the superiorities of MOFs in regulating fluorescent probes were presented. Despite the progress achieved in this field, there are other regulation effects of MOFs on fluorescent probes needing to be explored: (a) the solvent effect of fluorescent probes can be avoid *via* the microenvironment of MOF channels, so as to keep detection performances stable in different solvents; (b) fluorescent probes targeted at different analytes can be integrated into one MOF, so as to realize the detection of multiple substances; (c) fluorescent probes can be integrated into MOFs together with other probes, so as to achieve the multi-mode detection of analytes. It is desirably hoped that this review can provide a useful reference for the researchers interested in this subject.

Conflicts of interest

There are no conflicts to declare.

Acknowledgements

Thank the support from Hainan Provincial Natural Science Foundation of China (219QN154, 2019RC005), National Natural Science Foundation of China (21761010), the Research Start-up Fund Projects of Hainan University (KYQD(ZR)1926, KYQD(ZR) 1806), and the Opening Project of Key Laboratory of

Polyoxometalate Science (Ministry of Education), Northeast Normal University.

References

1 B. H. Wang, X. Lian and B. Yan, *Talanta*, 2020, **214**, 120856.
2 S. Kadian and G. Manik, *Food Chem.*, 2020, **317**, 126457.
3 L. J. Han, Y. J. Kong, G. Z. Hou, H. C. Chen, X. M. Zhang and H. G. Zheng, *Inorg. Chem.*, 2020, **59**, 7181–7187.
4 C. Ling, M. Cui, J. Chen, L. Xia, D. Deng, Y. Gu and P. Wang, *Talanta*, 2020, **215**, 120934.
5 W. L. Jiang, W. X. Wang, J. Liu, Y. F. Li and C. Y. Li, *Sens. Actuators, B*, 2020, **313**, 128054.
6 Z. J. Meng, L. Yang, C. X. Yao, H. Li, Y. Fu, K. X. Wang, Z. J. Qu and Z. H. Wang, *Dyes Pigm.*, 2020, **176**, 108208.
7 Q. Z. Yang, S. Z. Wang, D. Li, J. Y. Yuan, J. Xu and S. J. Shao, *Anal. Chim. Acta*, 2020, **1103**, 202–211.
8 S. T. Cai, C. Liu, X. J. Jiao, L. C. Zhao and X. S. Zeng, *J. Mater. Chem. B*, 2020, **8**, 2269–2274.
9 J. J. Yang, M. T. Fan, Y. Sun, M. Y. Zhang, Y. T. Xue, D. Z. Zhang, T. Wang and X. Y. Cui, *Sens. Actuators, B*, 2020, **307**, 127652.
10 P. Lesani, G. Singh, C. M. Viray, Y. Ramaswamy, D. M. Zhu, P. Kingshott, Z. Lu and H. Zreiqat, *ACS Appl. Mater. Interfaces*, 2020, **12**, 18395–18406.
11 P. C. Xing, D. Wu, J. S. Chen, J. M. Song, C. J. Mao, Y. H. Gao and H. L. Niu, *Analyst*, 2019, **144**, 2656–2661.
12 L. R. Liu, G. B. Zhu, W. Zeng, Y. H. Yi, B. H. Lv, J. J. Qian and D. P. Zhang, *Microchim. Acta*, 2019, **186**, 98–106.
13 W. X. Zhong, L. Z. Wang, S. M. Fang, D. W. Qin, J. H. Zhou, G. Yang and H. D. Duan, *RSC Adv.*, 2020, **10**, 3048–3059.
14 Y. Cai, J. K. Fang, B. F. Wang, F. S. Zhang, G. Shao and Y. J. Liu, *Sens. Actuators, B*, 2019, **292**, 156–163.
15 K. N. Zhu, T. Y. Z. Lv, T. Y. Qin, Y. Y. Huang, L. Wang and B. Liu, *Chem. Commun.*, 2019, **55**, 13983–13986.
16 L. Tao, C. J. Song, C. Y. Huo, Y. J. Sun, C. M. Zhang, X. H. Li, S. J. Yu, M. Y. Sun, B. Q. Jin, Z. J. Zhang and K. Yang, *Analyst*, 2016, **141**, 4933–4940.
17 L. J. Feng, G. J. Ren, S. A. Ding, F. X. Wang, W. T. Yang, Z. Q. Liang and Q. H. Pan, *Appl. Organomet. Chem.*, 2019, **33**, e5044.
18 D. X. Gu, W. T. Yang, F. X. Wang, M. L. Li, L. J. Liu, H. H. Li and Q. H. Pan, *Appl. Organomet. Chem.*, 2019, **33**, e5179.
19 L. Long, Y. Han, W. Liu, Q. Chen, D. Yin, L. Li, F. Yuan, Z. Han, A. Gong and K. Wang, *Anal. Chem.*, 2020, **92**, 6072–6080.
20 S. J. Li, P. P. Wang, W. Q. Feng, Y. H. Xiang, K. Dou and Z. H. Liu, *Chem. Commun.*, 2020, **56**, 1050–1053.
21 Z. Y. Qu, T. Yu and L. H. Bi, *Microchim. Acta*, 2019, **186**, 635.
22 X. L. Wu, P. L. Wu, M. Y. Gu and J. Xue, *Anal. Chim. Acta*, 2020, **1104**, 140–146.
23 S. H. Han, X. X. Yue, J. P. Wang, Y. Zhang, B. H. Wang and X. Z. Song, *New J. Chem.*, 2020, **44**, 4554–4557.
24 Y. L. Qiao, C. Y. Liu and X. W. Zheng, *Sens. Actuators, B*, 2018, **259**, 211–218.
25 X. F. Wu, X. H. Li, H. Y. Li, W. Shi and H. M. Ma, *Chem. Commun.*, 2017, **53**, 2443–2446.
26 Y. B. Gan, G. X. Yin, T. Yu, Y. Y. Zhang, H. T. Li and P. Yin, *Talanta*, 2020, **210**, 120612.
27 X. F. Wu, L. H. Li, W. Shi, Q. Y. Gong and H. M. Ma, *Angew. Chem., Int. Ed.*, 2016, **55**, 14728–14732.
28 S. J. Dong, J. S. Hu, X. L. Zhang and M. D. Zheng, *Inorg. Chem. Commun.*, 2018, **97**, 180–186.
29 M. Li, Z. H. Cui, S. R. Pang, L. K. Meng, D. X. Ma, Y. Li, Z. Shi and S. H. Feng, *J. Mater. Chem. C*, 2019, **7**, 11919–11925.
30 S. J. Dong, J. S. Hu, K. Wu and M. D. Zheng, *Inorg. Chem. Commun.*, 2018, **95**, 111–116.
31 Z. G. Song, R. T. K. Kwok, D. Ding, H. Nie, J. W. Y. Lam, B. Liu and B. Z. Tang, *Chem. Commun.*, 2016, **52**, 10076–10079.
32 V. J. Pastore, T. R. Cook and J. Rzayev, *Chem. Mater.*, 2018, **30**, 8639–8649.
33 S. Y. Zhang, Z. D. Yang, K. Gong, B. Xu, H. Mei, H. B. Zhang, J. X. Zhang, Z. X. Kang, Y. G. Yan and D. F. Sun, *Nanoscale*, 2019, **11**, 9598–9607.
34 D. Sompornpailin, C. Ratanatawanate, C. Sattayanon, S. Namuangruk and P. Punyapalakul, *Sci. Total Environ.*, 2020, **720**, 137449.
35 Y. F. Zhao, M. Y. Wan, J. P. Bai, H. Zeng, W. G. Lu and D. Li, *J. Mater. Chem. A*, 2019, **7**, 11127–11133.
36 D. A. Levenson, J. F. Zhang, B. S. Gelfand, S. P. Kammampata, V. Thangadurai and G. K. H. Shimizu, *Dalton Trans.*, 2020, **49**, 4022–4029.
37 Y. Zorlu, D. Erbahar, A. Cetinkaya, A. Bulut, T. S. Erkal, A. O. Yazaydin, J. Beckmann and G. Yucesan, *Chem. Commun.*, 2019, **55**, 3053–3056.
38 J. N. Hall and P. Bollini, *ACS Catal.*, 2020, **10**, 3750–3763.
39 A. Ghosh and G. Das, *Microporous Mesoporous Mater.*, 2020, **297**, 110039.
40 P. Tshuma, B. C. E. Makhubela, L. Ohrstrom, S. A. Bourne, N. Chatterjee, I. N. Beas, J. Darkwa and G. Mehlana, *RSC Adv.*, 2020, **10**, 3593–3605.
41 M. Pander, A. Zelichowska and W. Bury, *Polyhedron*, 2018, **156**, 131–137.
42 X. F. Liu, X. Y. Zhang, R. F. Li, L. Y. Du, X. Feng and Y. Q. Ding, *Dyes Pigm.*, 2020, **178**, 108347.
43 Y. F. Liu, D. y. Lin, W. T. Yang, X. Y. An, A. H. Sun, X. L. Fan and Q. H. Pan, *Microporous Mesoporous Mater.*, 2020, **303**, 110304.
44 C. Y. Sun, W. P. To, F. F. Hung, X. L. Wang, Z. M. Su and C. M. Che, *Chem. Sci.*, 2018, **9**, 2357–2364.
45 X. Ke, X. Q. Song, N. Q. Qin, Y. R. Cai and F. Ke, *J. Porous Mater.*, 2019, **26**, 813–818.
46 H. H. Li, F. X. Fu, W. T. Yang, L. Ding, J. X. Dong, Y. Yang, F. X. Wang and Q. H. Pan, *Sens. Actuators, B*, 2019, **301**, 127110.
47 Z. Sun, Y. Ling, S. G. Liu, Y. Z. Yang, X. H. Wang, Y. Z. Fan, N. B. Li and H. Q. Luo, *Inorg. Chem.*, 2019, **58**, 8388–8395.
48 X. J. Wu, F. Kong, C. Q. Zhao and S. N. Ding, *Analyst*, 2019, **144**, 2523–2530.
49 Y. Y. Wang, J. He, M. D. Zheng, M. D. Qin and W. Wei, *Talanta*, 2019, **191**, 519–525.
50 X. Fu, R. Lv, J. Su, H. Li, B. Y. Yang, W. Gu and X. Liu, *RSC Adv.*, 2018, **8**, 4766–4772.

51 Y. Q. Dong, J. H. Cai, Q. Q. Fang, X. You and Y. W. Chi, *Anal. Chem.*, 2016, **88**, 1748–1752.
52 J. Q. Liu, Y. Y. Zhao, X. L. Li, J. B. Wu, Y. D. Han, X. Zhang and Y. Xu, *Cryst. Growth Des.*, 2020, **20**, 454–459.
53 J. X. Wu and B. Yan, *Dalton Trans.*, 2017, **46**, 7098–7105.
54 X. Y. Xu and B. Yan, *J. Mater. Chem. C*, 2016, **4**, 1543–1549.
55 Y. J. Ma, G. H. Xu, F. D. Wei, Y. Cen, Y. S. Ma, Y. Y. Song, X. M. Xu, M. L. Shi, S. Muhammad and Q. Hu, *J. Mater. Chem. C*, 2017, **5**, 8566–8571.
56 Q. Q. Tan, R. R. Zhang, G. Y. Zhang, X. Y. Liu, F. L. Qu and L. M. Lu, *Anal. Bioanal. Chem.*, 2020, **412**, 1317–1324.
57 R. Jalili, A. Khataee, M. R. Rashidi and R. Luque, *Sens. Actuators, B*, 2019, **297**, 126775.
58 L. H. Xu, G. Z. Fang, J. F. Liu, M. F. Pan, R. R. Wang and S. Wang, *J. Mater. Chem. A*, 2016, **4**, 15880–15887.
59 Y. J. Ma, G. H. Xu, F. D. Wei, Y. Cen, X. M. Xu, M. L. Shi, X. Cheng, Y. Y. Chai, M. Sohail and Q. Hu, *ACS Appl. Mater. Interfaces*, 2018, **10**, 20801–20805.
60 X. M. Lin, G. M. Gao, L. Y. Zheng, Y. W. Chi and G. N. Chen, *Anal. Chem.*, 2014, **86**, 1223–1228.
61 C. Fan, X. X. Lv, F. J. Liu, L. P. Feng, M. Liu, Y. Y. Cai, H. Liu, J. Y. Wang, Y. L. Yang and H. Wang, *ACS Sens.*, 2018, **3**, 441–450.
62 A. Y. Zhang, C. Y. Fan, W. Sun, L. Chen, R. X. Shi, Y. Q. Cao and P. Yang, *J. Nanosci. Nanotechnol.*, 2019, **19**, 8088–8094.
63 F. Asadi, S. N. Azizi and M. J. Chaichi, *Mater. Sci. Eng., C*, 2019, **105**, 110058.
64 S. X. Yang, S. H. Lu, Y. Cheng, Z. X. Lu, X. L. Liu, Y. Qin, R. D. Zhao, L. Y. Zheng and Q. E. Cao, *Microporous Mesoporous Mater.*, 2020, **294**, 109959.
65 X. Hu, X. D. Liu, X. D. Zhang, H. X. Chai and Y. M. Huang, *Biosens. Bioelectron.*, 2018, **105**, 65–70.
66 K. Wang, N. Li, J. Zhang, Z. Q. Zhang and F. Q. Dang, *Biosens. Bioelectron.*, 2017, **87**, 339–344.
67 J. M. Yang, X. W. Hu, Y. X. Liu and W. Zhang, *Microporous Mesoporous Mater.*, 2019, **274**, 149–154.
68 H. H. Li, B. Fu, W. T. Yang, L. Ding, Y. Yang, J. X. Dong, F. X. Wang and Q. H. Pan, *Spectrochim. Acta, Part A*, 2020, **226**, 117575.
69 S. Let, P. Samanta, S. Dutta and S. K. Ghosh, *Inorg. Chim. Acta*, 2020, **500**, 119205.
70 D. Tian, X. J. Liu, R. Feng, J. L. Xu, J. Xu, R. Y. Chen, L. Huang and X. H. Bu, *ACS Appl. Mater. Interfaces*, 2018, **10**, 5618–5625.
71 X. Fu, H. Li, R. Lv, D. Hong, B. Y. Yang, W. Gu and X. Liu, *J. Solid State Chem.*, 2018, **264**, 35–41.
72 H. Q. Zheng, Y. N. Zhang, L. F. Liu, W. Wan, P. Guo, A. M. Nystrom and X. D. Zou, *J. Am. Chem. Soc.*, 2016, **138**, 962–968.
73 C. Gucuyener, J. van den Bergh, J. Gascon and F. Kapteijn, *J. Am. Chem. Soc.*, 2010, **132**, 17704–17706.
74 J. V. Morabito, L. Y. Chou, Z. H. Li, C. M. Manna, C. A. Petroff, R. J. Kyada, J. M. Palomba, J. A. Byers and C. K. Tsung, *J. Am. Chem. Soc.*, 2014, **136**, 12540–12543.
75 S. A. Moggach, T. D. Bennett and A. K. Cheetham, *Angew. Chem., Int. Ed.*, 2009, **48**, 7087–7089.
76 M. L. Li, W. T. Yang, P. F. Qiu, G. J. Ren, C. Y. Li, Z. Y. Chen, Y. H. Wang and Q. H. Pan, *J. Lumin.*, 2019, **205**, 380–384.
77 C. Cui, Q. B. Wang, C. H. Xin, Q. Y. Liu, X. Deng, T. T. Liu, X. H. Xu and X. M. Zhang, *Microporous Mesoporous Mater.*, 2020, **299**, 110122.
78 L. L. Xu, M. X. Wu, L. H. Zhao, H. Han, S. Q. Zhang, P. Y. Ma, Y. Sun, X. H. Wang and D. Q. Song, *Talanta*, 2020, **215**, 120892.
79 L. Yang, F. Wang, X. Z. Luo, X. J. Kong, Z. W. Sun and J. M. You, *Talanta*, 2020, **209**, 120517.
80 X. J. He, W. Xiong, L. Zhang, C. C. Xu, J. Y. Fan, Y. N. Qian, J. S. Wen, F. Ding and J. L. Shen, *Dyes Pigm.*, 2020, **174**, 108059.
81 J. M. Wang, Z. D. Teng, T. Cao, J. Qian, L. Zheng, Y. P. Cao, W. W. Qin and H. C. Guo, *Sens. Actuators, B*, 2020, **306**, 127567.
82 P. Ju, E. S. Zhang, L. Jiang, Z. Zhang, X. Y. Hou, Y. Q. Zhang, H. Yang and J. J. Wang, *RSC Adv.*, 2018, **8**, 21671–21678.
83 F. M. Wang, L. Zhou, W. P. Lustig, Z. C. Hu, J. F. Li, B. X. Hu, L. Z. Chen and J. Li, *Cryst. Growth Des.*, 2018, **18**, 5166–5173.
84 Y. Y. Jiang, L. B. Sun, J. F. Du, Y. C. Liu, H. Z. Shi, Z. Q. Liang and J. Y. Li, *Cryst. Growth Des.*, 2017, **17**, 2090–2096.
85 M. L. Li, G. J. Ren, F. X. Wang, Z. M. Li, W. T. Yang, D. X. Gu, Y. H. Wang, G. S. Zhu and Q. H. Pan, *Inorg. Chem. Front.*, 2019, **6**, 1129–1134.
86 Y. Zhao, L. Wang, N. N. Fan, M. L. Han, G. P. Yang and L. F. Ma, *Cryst. Growth Des.*, 2018, **18**, 7114–7121.
87 W. T. Yu, M. B. Luo, Y. X. Yang, H. Wu, W. Huang, K. Zeng and F. Luo, *J. Solid State Chem.*, 2019, **269**, 264–270.
88 S. M. Mirsoleimani-azizi, P. Setoodeh, S. Zeinali and M. R. Rahimpour, *J. Environ. Chem. Eng.*, 2018, **6**, 6118–6130.
89 D. N. Liu, C. J. Wang, Y. M. Xiao, C. Liu, D. Luo, Z. X. Zhu, S. Chen and Y. Y. Wang, *Inorg. Chem. Commun.*, 2020, **114**, 107773.
90 H. F. Zhang, M. Zhao and Y. S. Lin, *Microporous Mesoporous Mater.*, 2019, **279**, 201–210.
91 J. Li, Z. Wu, Q. Y. Duan, X. D. Li, Y. Li, H. Alsulami, M. S. Alhodaly, T. Hayat and Y. B. Sun, *J. Hazard. Mater.*, 2020, **393**, 122398.
92 Y. F. Li, X. L. Yan, X. Y. Hu, R. Feng, M. Zhou and D. Z. Han, *J. Porous Mater.*, 2020, **27**, 1109–1117.
93 Y. R. Son, S. G. Ryu and H. S. Kim, *Microporous Mesoporous Mater.*, 2020, **293**, 109819.
94 H. Yang, X. W. He, F. Wang, Y. Kang and J. Zhang, *J. Mater. Chem.*, 2012, **22**, 21849–21851.
95 J. A. Gee, J. Chung, S. Nair and D. S. Sholl, *J. Phys. Chem. C*, 2013, **117**, 3169–3176.
96 X. X. Gao, H. Y. Zhong, Y. Y. Zhang, Y. N. Yao, D. L. Chen and Y. B. He, *Eur. J. Inorg. Chem.*, 2020, 1683–1689.
97 A. H. Assen, Y. Belmabkhout, K. Adil, P. M. Bhatt, D. X. Xue, H. Jiang and M. Eddaoudi, *Angew. Chem., Int. Ed.*, 2015, **54**, 14353–14358.
98 J. Wang, J. J. Chen and T. Y. Xu, *Solid State Sci.*, 2019, **98**, 106032.

99 G. J. Ren, Z. M. Li, M. L. Li, Z. Q. Liang, W. T. Yang, P. F. Qiu, Q. H. Pan and G. S. Zhu, *Inorg. Chem. Commun.*, 2018, **91**, 108–111.
100 D. X. Gu, W. T. Yang, G. H. Ning, F. X. Wang, S. X. Wu, X. D. Shi, Y. H. Wang and Q. H. Pan, *Inorg. Chem.*, 2020, **59**, 1778–1784.
101 X. D. Zhang, G. J. Ren, M. L. Li, W. T. Yang and Q. H. Pan, *Cryst. Growth Des.*, 2019, **19**, 6308–6314.
102 W. X. Chen, P. Xie, X. X. Shan, H. Q. Zhao, Y. Wu, H. W. Zhou and X. L. Jin, *J. Mol. Struct.*, 2020, **1207**, 127822.
103 S. Z. Liu, D. Yang, Y. J. Liu, H. Pan, H. B. Chen, X. Z. Qu and H. M. Li, *Sens. Actuators, B*, 2019, **299**, 126937.
104 Z. H. Wang, D. Chen, B. L. Gu, B. Gao, Z. D. Liu, Y. S. Yang, Q. L. Guo, X. H. Zheng and G. Wang, *Diamond Relat. Mater.*, 2020, **104**, 107749.
105 S. A. Nsibande and P. B. C. Forbes, *RSC Adv.*, 2020, **10**, 12119–12128.
106 V. Glembockyte, M. Frenette, C. Mottillo, A. M. Durantini, J. Gostick, V. Strukil, T. Friscic and G. Cosa, *J. Am. Chem. Soc.*, 2018, **140**, 16882–16887.